Proceedings of the ASME 2009 Dynamic Systems and Control Conference
DSCC2009
October 12-14, 2009, Hollywood, California, USA

DSCC2009-2530

LOCOMOTION OF CIRCULAR ROBOTS WITH DIAMETRICALLY TRANSLATING LEGS

Eric Steffan
Department of Mechanical Engineering
Rochester Institute of Technology
Rochester, NY 14623
Email: ers2971@rit.edu

Tuhin Das
Department of Mechanical Engineering
Rochester Institute of Technology
Rochester, NY 14623
Email: tkdeme@rit.edu

ABSTRACT

In this paper, we develop an analytical basis for designing the locomotion of mobile robots with a spherical or circular core and equispaced diametral legs. The mechanism has resemblance with certain cellular locomotions. Locomotion is generated by actuation of the legs in the radial direction. Two elementary regimes of motion are first developed using the geometry of the mechanism. The overall motion of the robot is generated by repeated switching between the two regimes. The paper addresses both the kinematics and dynamics of the mechanism enabling the prediction of trajectories and computation of constraint and actuation forces. Simulation results are provided in support of the theory developed.

NOMENCLATURE

r	Radius of circular core $[m]$
r_1	Leg 1 extension $[m]$
r_2	Leg 2 extension $[m]$
r_3	Leg 3 extension $[m]$
L	Total length of each leg $[m]$
θ	Angle between leg 1 and ground $[deg]$
β	Angle between leg 2 and ground $[deg]$
R	Radius of circle described by center C - Phase I $[m]$
a	Distance between points of contact - Phase I $[m]$
$r_{1,0}$	Initial r_1 value - Phase I $[m]$
θ_0	Initial θ value - Phase I $[m]$
h	Height of center C at transition points $[m]$
M_d	Mass of core $[kg]$
M_r	Mass of each leg $[kg]$
I_c	Moment of inertia of core about C $[kg\,m^2]$
$I_{r,P}$, $I_{r,Q}$	Moment of inertia of leg about P and Q $[kg\,m^2]$
g	Earth's gravitational constant $[kg\,m/sec^2]$
μ_1	Coefficient of friction, leg 1
μ_2	Coefficient of friction, leg 2

INTRODUCTION

Mobile robotics is a vast area of research which has experienced rapid development in recent years. In the majority of robotic designs, mechanisms for self-propulsion have been inspired by various forms of locomotion that are observed in nature. In this paper we develop the analytical basis of designing the locomotion for a class of robotic mechanisms with linearly actuated legs. The robotic mechanism can be conceived as a spherical core with retractable legs oriented radially over the surface of the sphere. The robot is maneuvered by controlling the relative protrusion of the legs. A planar version of the mechanism is depicted in Fig.1. In this version we consider rectilinear motion of a circular core with radial legs. A salient feature of the mechanism is its overall shape-morphing ability. The leg protrusion and retraction are controlled to cause motive reaction forces while simultaneously providing a favorable mass unbalance aiding the locomotion.

The concept originates from earlier research conducted by Das et al. [1], [2] where the authors developed and analyzed internal propulsion mechanisms for spherical and circular robots. In the proposed designs in this paper, we design external propulsion mechanism while retaining the overall postural flexibility of the robot. The specific design is also prompted by *cellular locomotion of neutrophils*, or a type of white blood cell. Neutrophils use a simple yet effective mechanism, using expanding and contracting tentacles, to propel themselves forward in the presence of shear flow, [3], [4], and [5]. This observation demonstrates the potential feasibility of our concept of motion on a microscopic scale and motivates us to learn further about the underlying principles of neutrophil's cellular locomotion.

Designs with certain conceptual similarities are found in the literature. In [6] the authors discuss a hexapod insect-like mechanism with retractable legs. In this design, apart from the axial motion, each leg is allowed to swing. In [7] the authors design

walking robots with six compliant legs. Each leg is designed as a combination of three equispaced spring-loaded telescopic spokes forming a wheel, called 'wheg', where the discontinuities are used to gain footholds. In this design, each 'wheg' has rotational actuation about the center, in addition to the leg compliance. The Intelligent Mobility Platform with Active Spoke System (IMPASS), [8], [9], employ a mechanism consisting of two actuated-spoke wheels connected through a common axle. In addition to the radial spoke actuation, rotational torque is provided to the axle through a hub motor. An extra point of contact with ground is provided through a tail support. In [10], the authors discuss a rimless wheel with radially expanding legs, intended to be used on the three-wheel vehicle discussed in [11], or similar vehicles. The wheel consists of three spokes simultaneously actuated by a bevel gear in conjunction with ball screw and pinion assemblies. Radial extension is intended to catapult the vehicle over obstacles by expanding when a single spoke is in contact with the ground. The wheels can also be rotated via a central hub, allowing two degrees of freedom in the motion of the wheel. In comparison to the above designs, our proposed mechanism generates rectilinear locomotion exclusively through linear actuation of the legs. Furthermore, our mechanism uses one circular core instead of coaxial wheel pairs adopted in the above designs.

The proposed locomotion is designed with two distinct phases. In Phase I, mechanical energy is supplied into the system through controlled actuation of the legs. The momentum gained in the process is then used to complete Phase II which simply utilizes energy conservation. A pair of Phase I and II motion regimes are repeated to generate the overall locomotion. The energy losses incurred during a pair of Phase I and II motions are compensated in the next Phase I and so on. The analytical development is carried out with three equispaced legs. The choice of three legs is prompted by the use of three unbalance masses in the locomotion of a rolling disk in [1]. The mode of locomotion presented here, however, is applicable to an arbitrary number (potentially ≥ 2) of equispaced diametral legs.

SYSTEM DESCRIPTION

We conceptualize a robotic mechanism as shown in Fig.1. The mechanism consists of a circular core with N equispaced retractable legs. Each leg is along a diametral line of the circular core and can translate axially. The mechanism generates locomotion by controlling the radial motion of each leg. A unique aspect of the design is the effective shape morphing capability achieved by the robot, as shown by the dotted line in Fig.1. This happens due to the continuous change in the relative positions of the legs and is achieved in spite of the absence of a flexible outer covering or skin with an internal morphing mechanism. A natural concern is fouling of the legs. In a practical implementation this issue can be addressed by offsetting the legs in the lateral direction or by constructing each leg with two parallel bars. By choosing a different spacing between the bars of each leg, the legs will pass through one another without being offset and hence the later approach would maintain a balanced mass distribution in the lateral direction.

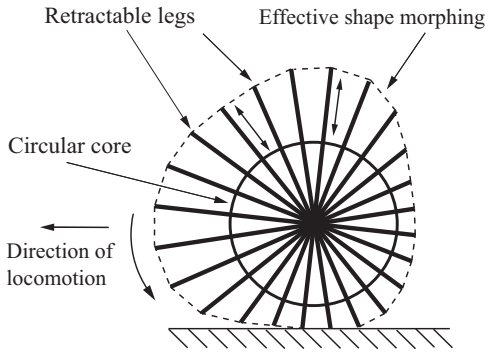

Figure 1. ROBOTIC MECHANISM CONCEPT

While Fig.1 represents the general concept, it is important to analyze the mechanism and design feasible modes of locomotion. Hence, in this paper, we study the specific case of three legs. The choice is motivated by our earlier research [1] where three unbalanced masses were used to generate rectilinear locomotion of a self-propelling rolling disk. A schematic diagram of the robot and its relevant coordinates is given in Fig.2(a).

MOTION ANALYSIS

We design the locomotion of the robot as an alternating sequence of two phases of motion. The two phases are as follows:

Phase I (Two point contact): The robot uses two contact points on the ground to propel itself, Fig.2(b).
Phase II (One point contact): The robot rolls about a fixed point of contact with the ground, Fig.2(c).

Motion Regimes

Phase I The motion in Phase I relies upon the kinematics obtained from the intrinsic geometry of the structure. From Fig.2(b), with P and Q as the two fixed points of contact and the geometric constraint $\angle PCQ = \angle PC'Q = 60^\circ$, the center C can only traverse a unique circular path. This can be easily proven and is also given by Euclid's inscribed angle theorem, as described in Fig.3. A relationship between r_1 and θ is established using the fact that $\beta = 120^\circ - \theta$:

$$r_1 + r = 2R\sin(120^\circ - \theta) \tag{1}$$

Noting that r is a constant and a and R are invariant during Phase I due to the fixed contact points P and Q, we have the following relations from Fig.3:

$$a = \sqrt{3}R = \frac{\sqrt{3}(r + r_{1,0})}{2\sin(120^\circ - \theta_0)} \tag{2}$$

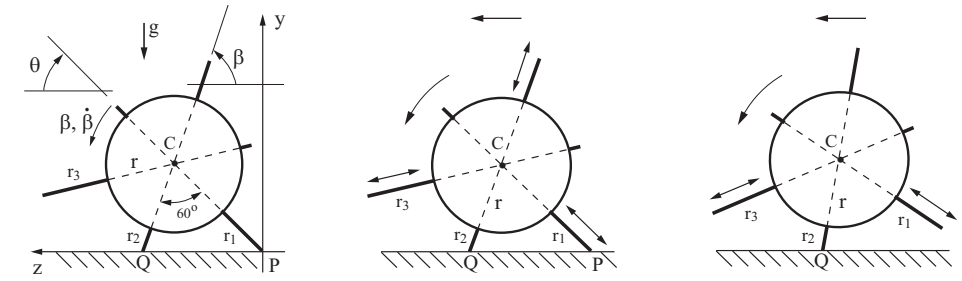

Figure 2. DIAGRAM OF THE ROBOTIC MECHANISM

where $r_{1,0}$ and θ_0 are the values of r_1 and θ at the initiation of Phase I. Differentiating Eqn.(1) with respect to time yields our velocity and acceleration constraint equations

$$\begin{aligned} \dot{r}_1 &= -2R\dot{\theta}\cos(120^\circ - \theta) \\ \ddot{r}_1 &= -2R\left[\ddot{\theta}\cos(120^\circ - \theta) + \dot{\theta}^2\sin(120^\circ - \theta)\right] \end{aligned} \tag{3}$$

Phase I motion can be implemented through linear actuators to generate controlled relative motion between the circular core and each leg.

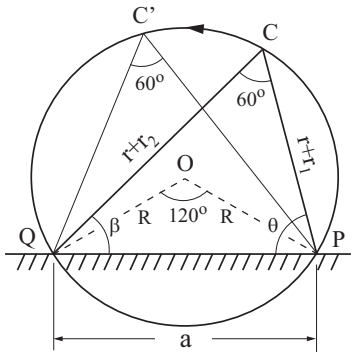

Figure 3. CIRCULAR TRAJECTORY OF CENTER DURING PHASE I

Phase II The motion in Phase II is a rotational motion as shown in Fig.2(c). The robot relies on its momentum to tip over the single point of contact. The center C again traverses a circular path during this phase. While the motion during one point contact can be designed in multiple ways, in our specific design there is no relative motion between the circular core and the supporting leg. Thus, the robot tips over Q as a rigid body and purely by virtue of its momentum. The rigid body mode can be implemented through a braking force applied by the restrictive linear actuator. During Phase II the robot therefore behaves as an inverted pendulum.

Combined Gait

The combined gait of the robot is generated by a repeating sequence of Phase I and Phase II motions. Such a repeating sequence can be designed in multiple ways. We consider the particular design shown in Fig.4 where the resulting motion of the robot's center is shown by the bold line. In Fig.4 the start and

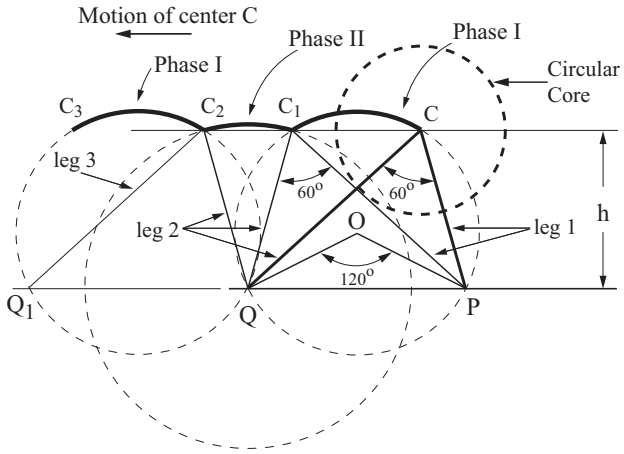

Figure 4. COMBINED GAIT

end of both phases occur at a constant vertical distance h from the ground, as shown in Fig.4. This admits not only the sequencing of Phases I and II with a continuous trajectory but also allows repetition of this sequence to generate a continuous motion. The motions $C - C_1$ and $C_1 - C_2$ correspond to Phase I and Phase II motions respectively. Note that since C, C_1, C_2 are at height h from the ground, CC_2QP forms a parallelogram. Therefore, C_2 provides an identical initial condition as C for Phase I motion. However, comparing C and C_2, note that legs 2 and 3 take the position of legs 1 and 2 during the second Phase I motion in Fig.4.

Note that the trajectory of the robot is completely defined by the values of the following variables at the beginning of Phase I, $\angle CPQ = \theta_0$, $CP = r + r_{1,0}$. It is observed that for feasible trajectories, $r_{1,0} \geq 0$ and $60^\circ \leq \theta_0 \leq 90^\circ$. The values $\theta_0 = 60^\circ$ and $\theta_0 = 90^\circ$ correspond to terminal scenarios where the motion is exclusively Phase II and Phase I respectively. While the latter scenario seems feasible in a practical scenario, the former is not, since a finite Phase I regime is required to input mechanical energy into the robot.

Phase Transitions

As noted earlier, while Phase I consists of controlled linear actuation, phase II motion relies completely on momentum. At the transition from Phase I to II, the relative motions of both legs 1 and 2 with respect to the circular core are stopped through a braking action. This causes the robot to tip over about the point Q in a rigid body mode. Thus, at the beginning of Phase II, the robot must have sufficient kinetic energy to undertake the intermediate height gain. It is important to note that at this transition, the abrupt braking of leg 2 will cause an *impulsive drop* in the velocity of center C. This is shown in Fig.5. The velocity of the center changes from v_{C1-} to v_{C1+}. Similarly, at the transition of Phase II to I, the velocity of center changes impulsively from v_{C2-} to v_{C2+}. At this later transition, the robot enters the Phase I regime where energy is again pumped into the system in a controlled manner through the linear actuators. From geometry of the combined gait and since mechanical energy is conserved during Phase II, $v_{C2-} = v_{C1+}$, and it can be shown that

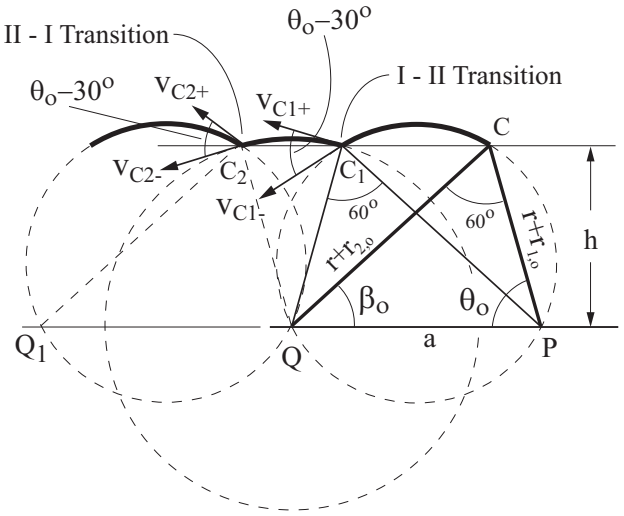

Figure 5. IMPULSIVE EFFECTS DURING PHASE TRANSITIONS

$$v_{C1+} = \cos(\theta_o - 30^\circ) v_{C1-}, \quad v_{C2+} = \cos(\theta_o - 30^\circ) v_{C2-} \tag{4}$$

From energy conservation and Eq.(4), it can be shown that Phase II will be feasible if

$$\begin{aligned} &0.5 I_c \dot{\beta}^2 + 0.5 M_d v_{C1+}^2 + M_d g (r + r_{1,o}) \sin\theta_o \geq M_d g (r + r_{1,o}) \\ &v_{C1-} \geq \sqrt{\frac{2(r+r_{1,o})^3 (1-\sin\theta_o) M_d g}{M_d (r+r_{1,o})^2 + I_c}} \cos(\theta_o - 30^\circ) \end{aligned} \tag{5}$$

In the above equation, we have assumed an idealized case where the entire mass of the robot is concentrated in the circular core and the legs of the robot are rigid and massless.

GEOMETRIC MOTION OPTIMIZATION

The combined gait can be optimized in several ways based on geometric or energy considerations. The purpose of the geometric optimization is to identify optimal θ_0 and/or $r_{1,0}$. We present two geometric optimizations that address optimal smoothness of the piecewise circular trajectory of the robot.

Scheme 1

In Fig.4, the points C, C_1, C_2, C_3, etc., all lie on a horizontal line, which is at a height h from the ground. The first scheme minimizes the maximum vertical departure of C from h during phases I and II, i.e., $\min(\max(\{q_{max,1}, q_{max,2}\})) \ \forall\ r_{1,0} \geq 0$ and $60^\circ \leq \theta_0 \leq 90^\circ$. $q_{max,1}$ and $q_{max,2}$ are defined as

$$q_{max,1} = y_{max,1} - h, \quad q_{max,2} = y_{max,2} - h \tag{6}$$

where, $y_{max,1}$ and $y_{max,2}$ are the maximum heights gained by the center C during phases I and II respectively. From Figs.4 and 5 and Eq.(2), we determine that

$$\begin{aligned} y_{max,1} &= R + R\sin 30^\circ = 1.5R = 3(r + r_{1,0}) / (4\sin(120^\circ - \theta_0)) \\ y_{max,2} &= r + r_{1,0} \end{aligned} \tag{7}$$

From Eqs.(6) and (7), we have

$$q_{max,1} = q_{max,2} \ \Rightarrow\ \theta_0 = 71.41^\circ \tag{8}$$

Note from Fig.5 that,

$$h = (r + r_{1,0}) \sin\theta_0 \tag{9}$$

Hence expressing $q_{max,1}$ and $q_{max,2}$ as

$$\begin{aligned} q_{max,1} &= y_{max,1} - h = 1.5R - 2R\sin(120^\circ - \theta_0)\sin\theta_0 \\ q_{max,2} &= y_{max,2} - h = 2R\sin(120^\circ - \theta_0)[1 - \sin\theta_0] \end{aligned} \tag{10}$$

taking the derivative of $q_{max,1}$ and $q_{max,2}$ with respect to θ_0 and using Eq.(2), we observe that for $60^\circ \leq \theta_0 \leq 90^\circ$

$$\begin{aligned} \tfrac{\partial q_{max,1}}{\partial \theta_0} &= -2R\sin(120^\circ - 2\theta_0) \\ &\quad + (1.5 - 2\sin(120^\circ - \theta_0)\sin\theta_0) \tfrac{R}{\tan(120^\circ - \theta_0)} \geq 0 \end{aligned} \tag{11}$$

and

$$\frac{\partial q_{max,2}}{\partial \theta_0} = -\cos\theta_0 (r + r_{1,0}) \leq 0 \tag{12}$$

This demonstrates that $q_{max,1}$ is an increasing function and $q_{max,2}$ is a decreasing function of θ_0 in the interval $60^\circ \leq \theta_0 \leq 90^\circ$. Therefore, $\min(\max(\{q_{max,1}, q_{max,2}\}))$ occurs at $\theta_0 = 71.41^\circ$ and is independent of the choice of $r_{1,0}$.

Scheme 2

The second scheme involves minimizing the total vertical departure of C from h, i.e., $\min(q_{max,1}+q_{max,2})$. Denoting $D = q_{max,1}+q_{max,2}$, from Eq.(10)

$$D = 1.5R + 2R\sin(120^\circ-\theta_0)\left[1-2\sin\theta_0\right] \tag{13}$$

Using Eq.(2) and taking the derivative of D with respect to θ_0 we obtain:

$$\begin{aligned}&\tfrac{\partial D}{\partial\theta_0} = 4\cos\theta_0\tan(120^\circ-\theta_0)\sin(120^\circ-\theta_0) - 1.5 = 0\\ &\Rightarrow\ \theta_0 = 68.08^\circ\end{aligned} \tag{14}$$

Therefore, $\min(q_{max,1}+q_{max,2})$ occurs at $\theta_0 = 68.08^\circ$ and is independent of the choice of $r_{1,0}$.

DYNAMIC ANALYSIS

Phase I

The motion in Phase I is governed by the constraint equations given in Eqs.(1) and (3). The dynamic equations during this phase will nevertheless be useful for estimation of linear actuation forces and required friction coefficients, which could be used as a design tool. We derive the dynamic equations using a Newtonian approach, with relevant free body diagrams shown in Fig.6. In Fig.6, F_{m1} and F_{m2} represent the linear actuation forces,

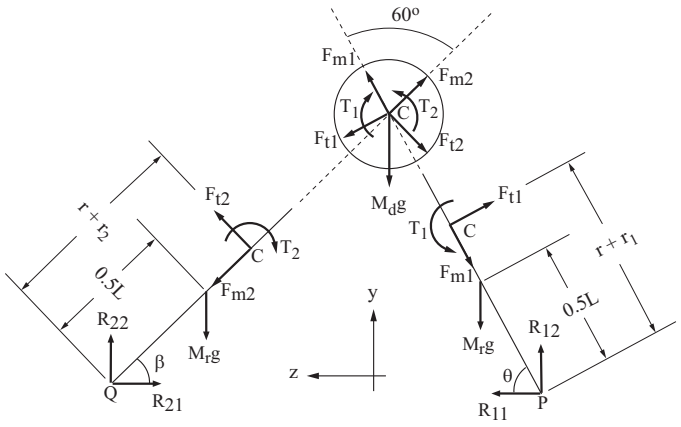

Figure 6. APPLIED AND CONSTRAINT FORCES - PHASE I

F_{t1} and F_{t2} represent the reaction forces tangential to the rotation of the legs, and T_1 and T_2 represent the reaction torques. The rest of the forces in Fig.6 are self-explanatory. The equations of motion for the circular core, the leg 1 (i.e. PC), and the leg 2 (i.e. QC), are

$$\begin{aligned}M_d\ddot{y}_c &= F_{m1}\sin\theta + F_{m2}\sin\beta - F_{t1}\cos\theta - F_{t2}\cos\beta - M_dg\\ M_d\ddot{z}_c &= F_{m1}\cos\theta - F_{m2}\cos\beta + F_{t1}\sin\theta - F_{t2}\sin\beta\\ I_c\ddot{\theta} &= T_1 - T_2\end{aligned} \tag{15}$$

$$\begin{aligned}M_r\ddot{y}_{r,1} &= -F_{m1}\sin\theta + F_{t1}\cos\theta + R_{12} - M_rg\\ M_r\ddot{z}_{r,1} &= -F_{m1}\cos\theta - F_{t1}\sin\theta + R_{11}\\ I_{r,P}\ddot{\theta} &= F_{t1}(r+r_1) - T_1 - (M_rgL/2)\cos\theta\end{aligned} \tag{16}$$

and

$$\begin{aligned}M_r\ddot{y}_{r,2} &= -F_{m2}\sin\beta + F_{t2}\cos\beta + R_{22} - M_rg\\ M_r\ddot{z}_{r,2} &= F_{m2}\cos\beta + F_{t2}\sin\beta - R_{21}\\ I_{r,Q}\ddot{\beta} &= F_{t2}(r+r_2) - T_2 - (M_rgL/2)\cos\beta\end{aligned} \tag{17}$$

where the coordinates of the center of the core and the midpoints of legs 1 and 2 are (y_c,z_c), $(y_{r,1},z_{r,1})$ and $(y_{r,2},z_{r,2})$ respectively. The following relationships are established from geometry:

$$\begin{aligned}\beta &= 120^\circ-\theta,\ \dot{\beta} = -\dot{\theta},\ \ddot{\beta} = -\ddot{\theta}\\ \ddot{y}_c &= \ddot{r}_1\sin\theta + 2\dot{r}_1\dot{\theta}\cos\theta + (r+r_1)\left[\cos\theta\ddot{\theta} - \sin\theta\dot{\theta}^2\right]\\ \ddot{z}_c &= \ddot{r}_1\cos\theta - 2\dot{r}_1\dot{\theta}\sin\theta - (r+r_1)\left[\sin\theta\ddot{\theta} + \cos\theta\dot{\theta}^2\right]\\ \ddot{y}_{r,1} &= (L/2)\cos\theta\ddot{\theta} - (L/2)\sin\theta\dot{\theta}^2\\ \ddot{z}_{r,1} &= -(L/2)\sin\theta\ddot{\theta} - (L/2)\cos\theta\dot{\theta}^2\\ \ddot{y}_{r,2} &= (L/2)\cos\beta\ddot{\beta} - (L/2)\sin\beta\dot{\beta}^2\\ \ddot{z}_{r,2} &= (L/2)\sin\beta\ddot{\beta} + (L/2)\cos\beta\dot{\beta}^2\end{aligned} \tag{18}$$

As mentioned earlier, in this paper we assume the legs to have no inertia, i.e. $M_r = I_{r,P} = I_{r,Q} = 0$.

Phase II

In Phase II, the robot undergoes pure rotation about point Q. There is no relative motion between the core and leg 2 and thus the motion occurs in a rigid body mode with the following dynamic equation of motion:

$$\left[I_c + M_d(r+r_{1,0})^2\right]\ddot{\beta} + M_dg(r+r_{1,0})\cos\beta = 0 \tag{19}$$

As in Phase I, it is important to determine the constraint forces to estimate the required coefficients of friction and the necessary actuator force to maintain the rigid body configuration. These quantities can be obtained by extracting the individual governing equations of the circular core and leg 2 from Eqs.(15) and (17) respectively. For Phase II, the equations of the core are

$$\begin{aligned}M_d\ddot{y}_c &= F_{m2}\sin\beta - F_{t2}\cos\beta - M_dg\\ M_d\ddot{z}_c &= -F_{m2}\cos\beta - F_{t2}\sin\beta\\ I_c\ddot{\beta} &= T_2\end{aligned} \tag{20}$$

The equations for leg 2 (CQ) are the same as in Eq.(17). In Phase II, since $y_c = (r+r_{1,0})\sin\beta$ and $z_c = -(r+r_{1,0})\cos\beta$, we have

$$\begin{aligned}\ddot{y}_c &= (r+r_{1,0})\left[\cos\beta\ddot{\beta} - \sin\beta\dot{\beta}^2\right]\\ \ddot{z}_c &= (r+r_{1,0})\left[\sin\beta\ddot{\beta} + \cos\beta\dot{\beta}^2\right]\end{aligned} \tag{21}$$

SIMULATION

Simulation results are provided to demonstrate the analysis presented in earlier sections. We present two sets of simulation results. In the first simulation, shown in Figs.7 and 8, $\theta_0 = 70^\circ$

and $r_{1,0} = 0.15$m. The simulation was run with the following constants: $r = 0.15$m, $M_d = 5$kg, $I_c = M_d r^2 = 0.0562$kg*m^2, $L = 0.6$m, $M_r = 0$. This leads to $\beta_0 = 50^\circ$ and $h = 0.282$m. For the simulations we imposed $\dot{r}_1 = 0.25$m/sec, and $\ddot{r}_1 = 0$ during Phase I. The initial conditions for Phase II are computed by the model considering the impulsive losses. Switching from Phase I to II occurs when $\theta = \beta_0$. Thereafter, over the course of Phase II, β varies from θ_0 to $180^\circ - \theta_0$. Transition from Phase II to I occurs when $\beta = 180^\circ - \theta_0$. The motion trajectories and the switching sequence are shown in Fig.7. The corresponding ac-

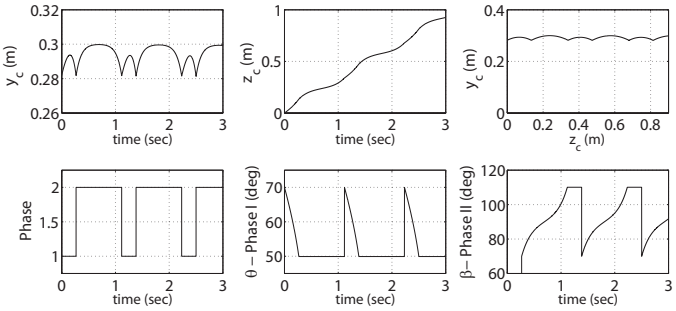

Figure 7. SIMULATION 1: MOTION TRAJECTORIES

tuator forces and coefficients of friction in Phases I and II are shown in Fig.8. The required friction coefficients are computed using a coulomb friction model. These computations were done using Eqs.(15), (16) and (17) with a particle assumption for the core and its rotational inertia was neglected. This gave unique values for F_{m1} and F_{m2}. In our ongoing work, we remove this assumption and compute the actuator forces through a pseudo-inverse. Note that the change in sign of μ_2 during Phase II is due to a reversal in the direction of friction force as the robot tips over point Q. In Fig.9, we show the motion trajectories with $\theta_0 = 80^\circ$.

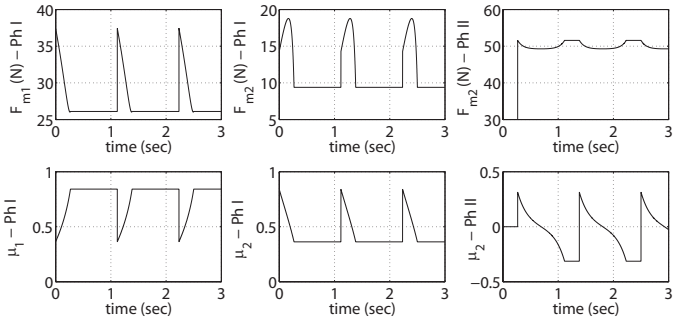

Figure 8. SIMULATION 1: ACTUATOR FORCES AND FRICTION COEFFICIENTS

For this simulation, the values of $r_{1,0}$, $\dot{r}_1$, $\ddot{r}_1$ and the constants are chosen to be same as in the first simulation. A noticeable difference between the two simulations is the relative prominence of Phase I and II. In the former, Phase II is more prominent than the latter as the net tipping angle is 40° in the former and 20° in the latter. Phase I involves a net rotation of 40° in the latter simulation and 20° in the former and hence is more prominent in the second simulation.

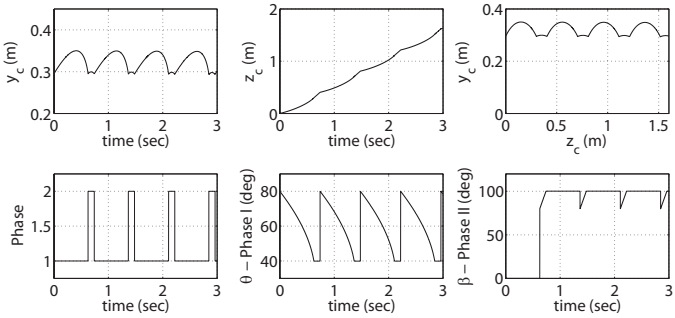

Figure 9. SIMULATION 2: MOTION TRAJECTORIES

CONCLUSION

In this paper we have designed a method of locomotion for circular robots with radially protruding legs. Motion is generated using an alternating sequence of two elementary maneuvers. In the resulting motion, the robot center describes piecewise circular arcs. The inherent flexibility of motion planning allows geometric trajectory optimization. The required actuation forces and friction properties are investigated through a dynamic analysis. While the proposed locomotion assumes no-slip, slipping conditions can be allowed under a modification of this locomotion that is currently being pursued by the authors. The mechanism is designed for three protruding legs, however the principles and motion regimes are applicable to an N legged circular robot. Simulation results are presented to confirm the analytical approach. A prototype with a cylindrical core is currently being built. While actuator bandwidth will not likely pose a limitation due to motion feasibility at low speeds, coordination and distribution of actuator forces will potentially pose challenges in the implementation. With some modifications, the idea could be extended to the spherical case.

ACKNOWLEDGMENT

The authors would like to thank Dr. Kathleen Lamkin-Kennard, Assistant Professor of Mechanical Engineering at RIT, for helpful discussions on cellular locomotion mechanisms.

REFERENCES

[1] Das, T., and Mukherjee, R., 2001. "Dynamic analysis of rectilinear motion of a self propelling disk with unbalance masses". *Journal of Applied Mechanics,* **68**, pp. 58–66.

[2] Das, T., and Mukherjee, R., 2004. "Exponential stabilization of the rolling sphere". *Automatica,* **40**, pp. 1877–1889.

[3] Mizuno, T., Kagami, O., Sakai, T., and Kawasaki, K., 1996. "Locomotion of neutrophil fragments occurs by graded radial extension". *Journal of Cell Motility and the Cytoskeleton,* **35**, pp. 289–297.

[4] King, M. R., Sumagin, R., Green, C. E., and Simon, S. I., 2005. "Rolling dynamics of a neutrophil with redistributed l. selectin". *Journal of Mathematical Biosciences,* **194**, pp. 71–79.

[5] Alon, R., and Ley, K., 2008. "Cells on the run: shear regulated integrin activation in leukocyte rolling and arrest on endothelial cells". *Journal of Current Opinion in Cell Biology,* **20**, pp. 1–8.

[6] Beer, R. D., Quinn, R. D., Chiel, H. J., and Ritzmann, R. E., 1997. "Biologically inspired approaches to robotics". *Communications of the ACM,* **40**(3), pp. 30–38.

[7] Schroer, R. T., Boggess, M. J., Bachmann, R. J., Quinn, R. D., and Ritzmann, R. E., 2004. "Comparing cockroach and whegs robot body motion". *IEEE Conference on Robotics and Automation, New Orleans*.

[8] Laney, D., and Hong, D., 2005. "Kinematic analysis of a novel rimless wheel with independently actuated spokes". *Proceedings of the ASME International Design Engineering Technical Conferences and Computer and Information in Engineering Conferences*, pp. 609–614.

[9] Kimmel, S., 2008. "Considerations for and implementations of deliberative and reactive motion planning strategies for the novel actuated rimless spoke wheel robot impass in the two-dimensional sagittal plane". *MS Thesis, Virginia Polytechnic Institute and State University*.

[10] Agrawal, S. K., and Yan, J., 2004. "Rimless wheel with radially expanding spokes: Dynamics, impact, and stable gait". *Proceedings of the 2004 IEEE International Conference on Robotics and Automation,* **4**, pp. 3240–3244.

[11] Agrawal, S. K., and Yan, J., 2003. "A three-wheel vehicle with expanding wheels: Differential flatness, trajectory planning, and control". *Proceedings of the 2003 IEEE/RJS International Conference on Intelligent Robots and Systems,* **2**, pp. 1450–1455.